Revisiting Hydrophobic Mismatch with Free Energy Simulation Studies of Transmembrane Helix Tilt and Rotation

Taehoon Kim and Wonpil Im*
Department of Molecular Biosciences and Center for Bioinformatics, The University of Kansas, Lawrence, Kansas

ABSTRACT Protein-lipid interaction and bilayer regulation of membrane protein functions are largely controlled by the hydrophobic match between the transmembrane (TM) domain of membrane proteins and the surrounding lipid bilayer. To systematically characterize responses of a TM helix and lipid adaptations to a hydrophobic mismatch, we have performed a total of 5.8-μs umbrella sampling simulations and calculated the potentials of mean force (PMFs) as a function of TM helix tilt angle under various mismatch conditions. Single-pass TM peptides called WALP*n* ($n = 16$, 19, 23, and 27) were used in two lipid bilayers with different hydrophobic thicknesses to consider hydrophobic mismatch caused by either the TM length or the bilayer thickness. In addition, different flanking residues, such as alanine, lysine, and arginine, instead of tryptophan in WALP23 were used to examine their influence. The PMFs, their decomposition, and trajectory analysis demonstrate that 1), tilting of a single-pass TM helix is the major response to a hydrophobic mismatch; 2), TM helix tilting up to ~10° is inherent due to the intrinsic entropic contribution arising from helix precession around the membrane normal even under a negative mismatch; 3), the favorable helix-lipid interaction provides additional driving forces for TM helix tilting under a positive mismatch; 4), the minimum-PMF tilt angle is generally located where there is the hydrophobic match and little lipid perturbation; 5), TM helix rotation is dependent on the specific helix-lipid interaction; and 6), anchoring residues at the hydrophilic/hydrophobic interface can be an important determinant of TM helix orientation.

INTRODUCTION

The transmembrane (TM) domain of most membrane proteins consists of one or multiple helices, and their interactions with surrounding lipids are important determinants for membrane protein structure and function. Understanding of membrane protein functions thus requires not only the protein structural information, but also information on how the lipid environments affect protein structure and organization. The match between the hydrophobic length of the TM domain and that of the lipid bilayer has been recognized as a central feature in protein-lipid interactions and bilayer regulation of membrane protein functions (1). Responses to an energetically unfavorable hydrophobic mismatch include conformational changes of the TM domain, lipid adaptations by changes in bilayer thickness and lipid chain order, and TM helix association (2). In particular, the changes in TM helix tilt, kink, and rotation angles to relieve any mismatch are often considered key conformational changes implicated in a switch between active and inactive conformations of membrane proteins (3–5). However, structural and dynamic changes of the TM domain in response to a hydrophobic mismatch as well as molecular forces governing such changes remain to be fully understood at the atomic level. In particular, given the abundance of membrane proteins with a single-pass TM helix and their association and conformational changes involved in TM-induced signaling (6,7), it is important and challenging to understand such properties quantitatively.

Mainly due to experimental difficulties associated with membrane proteins of multiple TM helices, our understanding of hydrophobic mismatch effects is mostly based on studies using various single-pass TM helices in model lipid bilayers. The responses to a hydrophobic mismatch have been systematically investigated by changing the hydrophobic length of TM helices or the hydrophobic thickness of lipid bilayers. In particular, designed TM helical peptides, such as WALP and KALP containing polyleucine/alanine flanked by tryptophan or lysine (Table 1), have been extensively used both in experimental (1,8–13) and computational (14–19) studies to characterize a main response to a hydrophobic mismatch as well as the role of peptide-lipid interactions. In the case of a single-pass TM helix, helix tilting is generally considered the main response to a hydrophobic mismatch with minimum perturbation of lipid bilayers (18,20). Recently, based on the potential-of-mean-force (PMF) calculation as a function of WALP19's tilt angle in a dimyristoylphosphatidyl-choline (DMPC) bilayer, Lee and Im (18) have provided novel insights (to our knowledge) into the driving forces of TM helix tilting in the lipid bilayer: a thermally accessible tilt region of a single-pass TM helix is governed by the intrinsic entropic contribution arising from helix precession (area) around the membrane normal and the helix-lipid interactions that could be TM sequence- and length-specific.

The aim of this work is to provide in-depth understanding of detailed interplays of specific helix-lipid interactions in TM helix tilting and lipid adaptations under various hydrophobic mismatch conditions. We have performed a total of 5.8-μs umbrella sampling molecular dynamics (MD)

Submitted February 12, 2010, and accepted for publication April 8, 2010.

*Correspondence: wonpil@ku.edu

Editor: Nathan Andrew Baker.

0006-3495/10/07/0175/9 $2.00

doi: 10.1016/j.bpj.2010.04.015

TABLE 1 Amino acid sequences of WALP*n* (*n* = 16, 19, 23, and 27) and *X*ALP23 (*X* = A, K, and R) peptides

Peptide	Sequence*	TM hydrophobic length (Å)†
WALP16	GWW(**LA**)$_5$WWA	15.0
WALP19	GWW(**LA**)$_6$**L**WWA	19.5
WALP23	GWW(**LA**)$_8$**L**WWA	25.5
WALP27	GWW(**LA**)$_{10}$**L**WWA	31.5
AALP23	GAA(**LA**)$_8$**LAAA**	31.5
KALP23	GKK(**LA**)$_8$**L**KKA	25.5
RALP23	GRR(**LA**)$_8$**L**RRA	25.5

*The N-terminus of each peptide is blocked by the acetyl group and its C-terminus by the *n*-methyl amide group.
†The lengths are measured in the hydrophobic region (bold) with an assumption of an ideal α-helix.

simulations (21) to calculate the PMFs of various single-pass TM helices as a function of their tilt and rotation angles (22,23) and analyzed the resulting PMFs by the free energy decomposition technique (18,22).

First, we used WALP*n* (*n* = 16, 19, 23, and 27; Table 1) in DMPC bilayers to determine the influence of the TM hydrophobic length on TM helix orientation and lipid adaptations. Second, the results in DMPC were compared with those in palmitoyloleoylphosphatidyl-choline (POPC) bilayers to characterize the influence of the bilayer hydrophobic thickness on TM helix orientation and lipid adaptations. Third and finally, we used alanine, lysine, and arginine as a flanking residue instead of tryptophan in WALP23 in DMPC to examine the influence of various anchoring residues on TM helix orientation and lipid adaptations (12). The PMFs, their decomposition, and trajectory analysis are discussed and generalized in terms of responses of a TM helix and lipid adaptations to various hydrophobic mismatch conditions.

METHODS

Defining the tilt and rotation angles

The orientation of a TM helix is defined by its tilt (τ) and rotation (ρ) angles. With the *Z* axis parallel to the membrane normal, τ is defined as the angle between the helical principal axis and the unit vector along the *Z* axis (22). To define ρ, both the internal and external references have to be defined (Fig. 1). The internal reference is given by the vector pointing from the helical axis to Cα atom of Leu^{14} in all WALP peptides except WALP16/19. Because the position of Leu^{14} in WALP16/19 is too close to the C-terminus, the flexibility of which makes it difficult to define ρ, we instead used Ala^7 (WALP16) and Leu^{10} (WALP19), which are at a similar position to Leu^{14} on the helical wheel projection. With the unit vector along the *Z* axis as the external reference, ρ is then defined as the angle between the projections of such reference vectors on the plane made by the second and third helical principal axes. Detailed expressions can be found in our previous works (22,24).

Umbrella sampling simulations

The sequence of each peptide studied in this work is given in Table 1. Using the input scripts from the Membrane Builder module (25,26) in CHARMM-GUI (http://www.charmm-gui.org) (27), each peptide with an ideal α-helical conformation ($\phi = -57.8°$; $\psi = -47.0°$) was inserted into a pre-equilibrated lipid bilayer of 72 DMPC (or POPC) and water molecules with $\tau = 0°$ and its center at $Z = 0$. Four chloride ions were added to neutralize the KALP23 and RALP23 systems. To relax the uncorrelated initial systems, 400-ps equilibration was performed with harmonic restraints on heavy atoms. The number of individual components and each system size are listed in Table S1 in the Supporting Material. The snapshots of each system at $\tau = 0°$ are shown in Fig. 2.

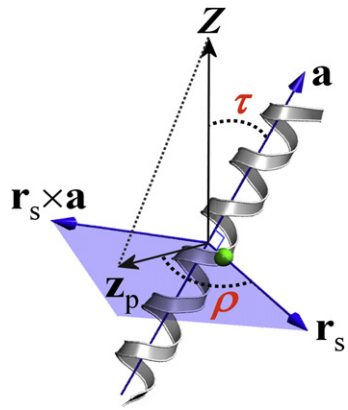

FIGURE 1 The definition of helix tilt (τ) and rotation (ρ). The value ρ is defined as the angle between the perpendicular vector (r_s) from the helical axis (*a*) to the selected Cα atom (*green circle*) and the projection vector (z_p) of the *Z* axis onto the plane (*light blue*) made by the second and third principal axes. The sign of the rotational angle becomes positive if $z_p \times r_s$ is in the opposite direction to *a*, or negative otherwise.

To perform umbrella sampling MD simulations as a function of TM helix tilt, an initial structure at each window was generated by tilting the helix sequentially from 0° to a specific maximum angle by 1° every 100 ps. The total number of windows and the maximum τ are listed in Table S1. Each window was then subjected to 1-ns equilibration followed by 10- or 12.5-ns production. The force constants of the helix tilt restraint potential (22) were set to 2000 and 6000 kcal/(mol·rad^2) (18) for equilibration and production, respectively. All calculations were performed using the biomolecular simulation program CHARMM (28) with the all-atom parameter set PARAM22 for protein (29) including the dihedral cross-term corrections (30) and a modified TIP3 water model (31), as well as recently optimized lipid parameters (32). The cross-sectional areas of DMPC and POPC were set to 60.7 Å^2 and 68.3 Å^2 at 303.15 K (33), respectively. Following the same protocol in the previous PMF calculation of WALP19 (18), a time-step of 2 fs was used with the SHAKE algorithm (34), and the constant temperature (303.15 K) and pressure (1 atm along the *Z*-direction) were maintained by the Nosé-Hoover method (35) and the Langevin-piston algorithm (36), respectively, for the NPAT (constant pressure, surface area, and temperature) dynamics. We used the same options for nonbonded interactions in the input scripts provided by the CHARMM-GUI Membrane Builder (25,26).

The PMF, $W(\tau)$, as a function of τ was calculated by integrating the reversible work done by the mean force, $-\langle F(\tau)\rangle_\tau$, along τ;

$$\frac{dW(\tau)}{d\tau} = -\langle F(\tau)\rangle_\tau = \left\langle \frac{\partial U(\mathbf{r})}{\partial \tau} - k_B T \frac{\partial \ln |J|}{\partial \tau} \right\rangle_\tau, \quad (1)$$

where $U(\mathbf{r})$ is the potential energy of the system, $|J|$ is the determinant of the Jacobian related to the transformation of the Cartesian coordinate into the generalized coordinate τ, and k_B is the Boltzmann constant. To examine the PMF convergence, the trajectory in each window was sequentially divided into every 1-ns duration. The PMFs were then calculated from each subtrajectory. When the PMF was constructed using the last 8-ns trajectory, even the highest standard deviation does not exceed ±2.2 kcal/mol (in the RALP23/DMPC system), illustrating that the calculated PMFs are well converged. The largest standard deviation of the PMFs occurs at either energetically unfavorable small or large tilt angle region (Fig. 3).

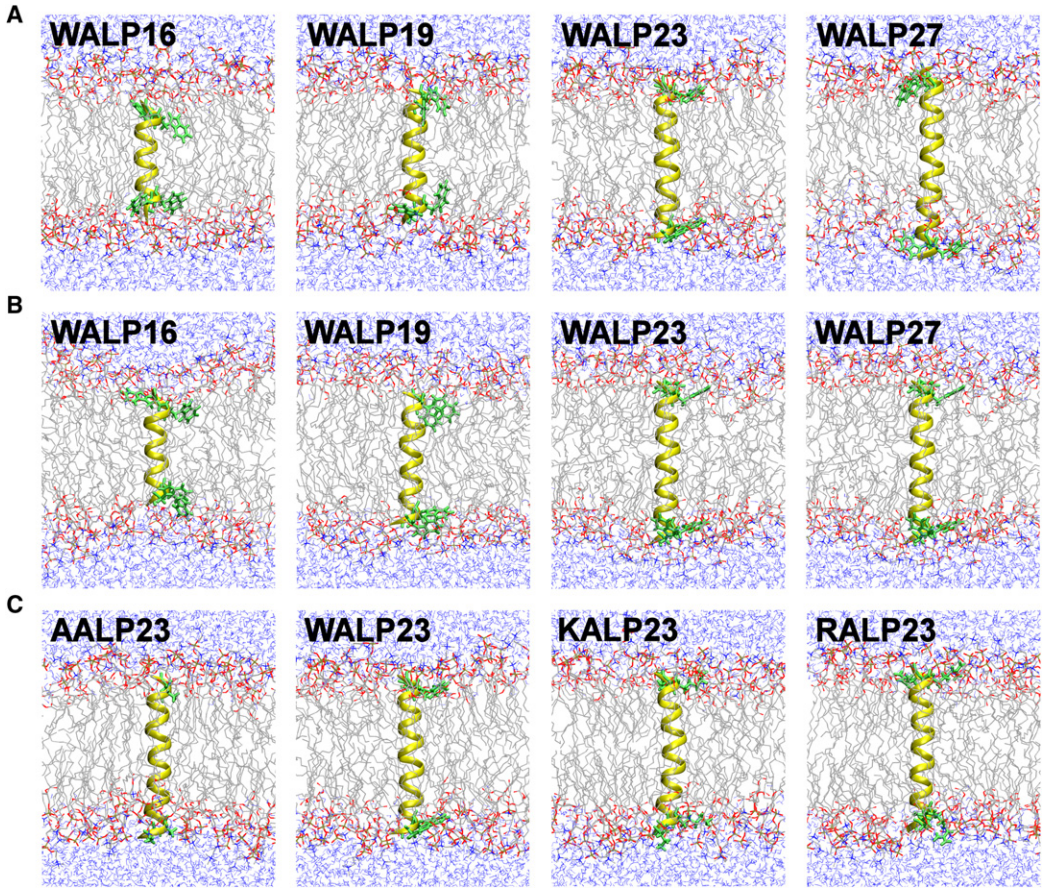

FIGURE 2 Molecular graphic view of the last snapshot in (*A*) WALP*n*/DMPC, (*B*) WALP*n*/POPC, and (*C*) *X*ALP23/DMPC systems at $\tau = 0^\circ$ (the helix in *yellow*, anchoring residues in *green*, lipid tails in *gray*, and water molecules in *blue*).

RESULTS AND DISCUSSION

Influence of hydrophobic length of TM helices

Tilting of a TM helix in a bilayer is affected by its TM hydrophobic length (L_{TM}) and the bilayer hydrophobic thickness ($L_{bilayer}$) whose difference can cause either positive ($L_{TM} > L_{bilayer}$) or negative ($L_{TM} < L_{bilayer}$) hydrophobic mismatch. In a DMPC bilayer with $L_{bilayer} \approx 23$ Å (10), WALP16/19 and WALP23/27 at $\tau = 0^\circ$ are under negative and positive mismatch conditions, respectively (see L_{TM} in Table 1). Fig. 3 *A* shows the total PMFs of the WALP*n*/DMPC systems as a function of τ. The detailed information about the minimum-PMF tilt angle (τ_{min}) and the free energy change from $\tau = 0^\circ$ to τ_{min}, $\Delta W(0 \rightarrow \tau_{min})$ in each system is summarized in Table 2. As L_{TM} increases, τ_{min} increases, $\Delta W(0 \rightarrow \tau_{min})$ decreases, and the thermally accessible tilt region becomes wider, clearly illustrating that it is energetically more favorable for TM helices of longer L_{TM} to have larger τ_{min} in order to maximize the hydrophobic match. In the case of WALP23, its τ_{min} is similar to the average tilt

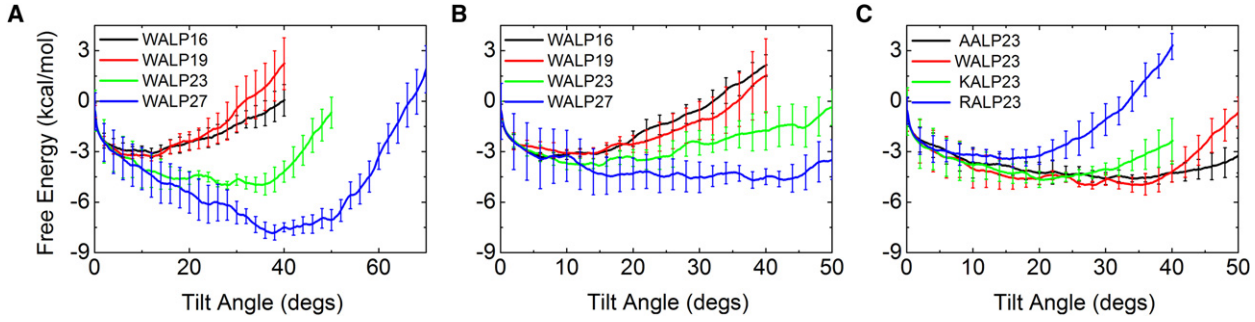

FIGURE 3 The total PMFs as a function of τ in (*A*) WALP*n*/DMPC, (*B*) WALP*n*/POPC, and (*C*) *X*ALP23/DMPC systems.

TABLE 2 The summary of the PMF in each system

System: peptide/lipid	Minimum-PMF tilt angle/ $\Delta W(0\rightarrow\tau_{min})$ (kcal/mol)	Thermal-accessible tilt range
WALP16/DMPC	12.1°/−3.09 ± 0.27	2.6° ~ 19.4°
WALP19/DMPC	12.1°/−3.30 ± 0.24	3.1° ~ 16.1°
WALP23/DMPC	28.1°/−4.99 ± 0.21	14.4° ~ 39.0°
WALP27/DMPC	43.3°/−7.45 ± 0.51	32.3° ~ 50.7°
WALP16/POPC	6.4°/−3.33 ± 0.21	3.3° ~ 17.4°
WALP19/POPC	12.5°/−3.14 ± 0.29	2.7° ~ 19.9°
WALP23/POPC	14.9°/−3.83 ± 0.28	6.7° ~ 25.6°
WALP27/POPC	38.2°/−4.70 ± 0.49	13.7° ~ 46.3°
AALP23/DMPC	34.2°/−4.60 ± 0.19	16.5° ~ 44.5°
KALP23/DMPC	20.7°/−4.68 ± 0.41	13.6° ~ 29.3°
RALP23/DMPC	15.6°/−3.44 ± 0.53	4.0° ~ 22.4°

($\tau = 33.5°$) from the recent multiple MD trajectories (16). Also, although the lipid types are different, the large τ_{min} from the PMF appears to be consistent with the recent fluorescence spectroscopy experiment (20) that shows much larger tilt angle of WALP23 ($\tau = 24° \pm 5°$) in a DOPC membrane than the tilt angle ($\tau = 4.4°$~$8.2°$) estimated from solid-state ^{2}H-NMR quadrupolar splitting measurements (12,13).

TM helix tilting is governed by the intrinsic entropic contribution ($W_{entropy}$) arising from helix precession (area) around the membrane normal and the specific helix-lipid interactions (W_{int}) (18). To determine detailed interplays of underlying molecular forces in TM helix tilting in the WALP*n*/DMPC systems, the total PMF of each system was decomposed into W_{int} and $W_{entropy}$ based on Eq. 1. It should be noted that W_{int} also includes the contribution from the helix conformational changes that resulted from the helix-lipid interactions. As shown in Fig. 4, *A* and *B*, under the negative mismatch condition such as the WALP16/19 systems, it is evident that tilting up to τ_{min} is driven by

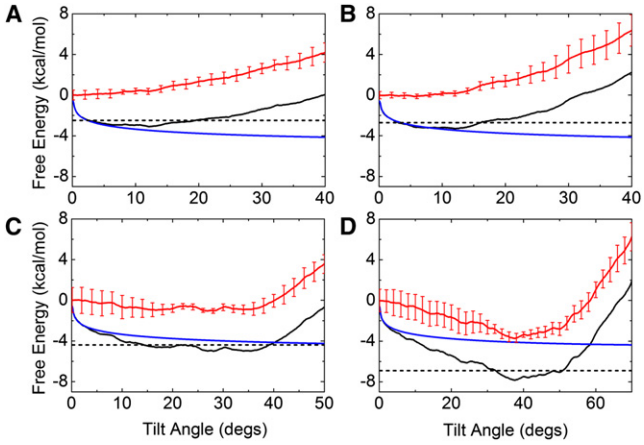

FIGURE 4 Decomposition of the total PMF (*black*) into the helix-lipid interaction (W_{int}: *red*) and the entropic contribution ($W_{entropy}$: *blue*) in (*A*) WALP16, (*B*) WALP19, (*C*) WALP23, and (*D*) WALP27 in DMPC bilayers. The thermally accessible tilt region is indicated by the black-dashed line.

$W_{entropy}$. After τ_{min}, W_{int} makes the dominant contribution to the increase of the PMFs. These results clearly explain the microscopic driving forces of previous MD simulation observations that a short TM helix can tilt up to ~10° in a membrane even under a negative mismatch condition (14). As L_{TM} increases, such as WALP23/27 in Fig. 4, *C* and *D*, the W_{int} contribution to the total PMF becomes more significant to maximize the hydrophobic match and provides additional driving forces for TM helix tilting.

The W_{int} contribution can be further characterized in terms of lipid adaptations, hydrophobic match, and helix conformational changes as a function of τ. In particular, it has been postulated that the lipids near an integral membrane protein would change their hydrophobic length or that the protein itself undergoes conformational changes to maximize the hydrophobic match (i.e., to minimize the energy penalty of exposing nonpolar residues to aqueous solution) (1). The present umbrella sampling simulation trajectory provides an excellent resource to quantify such changes at the atomic level, which would be difficult to measure in normal MD simulations because of limited sampling along TM helix orientations. In this study, the local lipid adjustment is quantified by

$$\Delta L^{adaptation} = \left\langle L_{bilayer}^{contact} \right\rangle - \left\langle L_{bilayer}^{bulk} \right\rangle,$$

where $\langle L_{bilayer}^{contact} \rangle$ and $\langle L_{bilayer}^{bulk} \rangle$ are the average hydrophobic thicknesses of contact and bulk lipid bilayers, respectively. $L_{bilayer}$ is defined as an average distance between the acyl chain C2 carbon atoms in both leaflets (10). A lipid molecule that has any of its heavy atoms within 4 Å from the helix heavy atoms is classified as a contact lipid, otherwise as a bulk one. Therefore, the negative $\Delta L^{adaptation}$ indicates a local membrane thinning and the positive $\Delta L^{adaptation}$ a local membrane thickening with respect to the bulk lipid bilayer. $\Delta L^{adaptation}$ as a function of τ in Fig. 5 *A* clearly shows that the local lipids respond differently to different hydrophobic mismatch conditions. For WALP16/19 that are under the negative mismatch ($L_{bilayer} > L_{TM}$) at $\tau = 0°$, the local membrane thinning ($\Delta L^{adaptation} < 0$) is apparent and $\Delta L^{adaptation}$ slightly decreases as τ increases. In contrast, for WALP23/27 that are under the positive mismatch ($L_{bilayer} < L_{TM}$) at $\tau = 0°$, the local membrane thickening ($\Delta L^{adaptation} > 0$) occurs at small tilt angles, but becomes reduced as τ increases and disappears at ~τ_{min} where there is little local lipid perturbation due to the hydrophobic match (see below). After τ_{min}, to maximize hydrophobic match, the contact lipids become thinner ($\Delta L^{adaptation} < 0$) because the effective L_{TM} is reduced as τ increases. Fig. 6 schematically illustrates how the local lipid adaptations occur at $\tau = 0°$, $\tau \approx \tau_{min}$, and $\tau > \tau_{min}$, based on Fig. 5 *A*.

To quantify the extent of the hydrophobic match as a function of τ, we calculated the difference between the effective L_{TM} (13) and $\langle L_{bilayer}^{contact} \rangle$, i.e.,

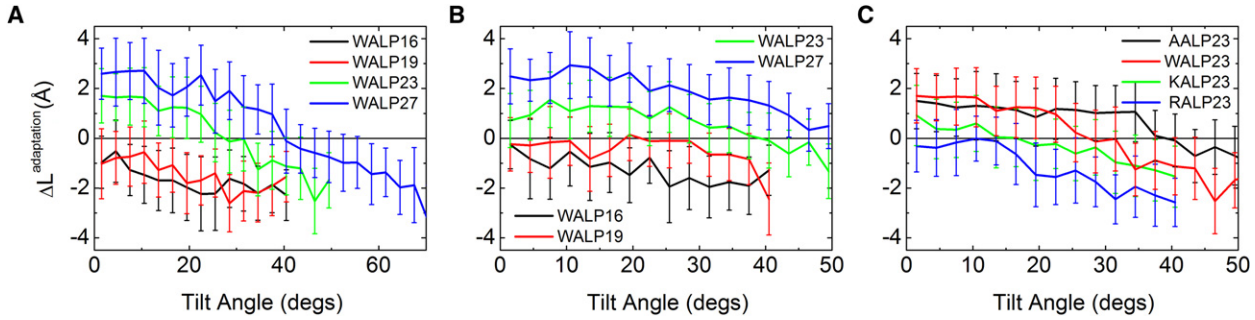

FIGURE 5 Local lipid adjustment ($\Delta L^{\text{adaptation}}$) as a function of τ in (*A*) WALP*n*/DMPC, (*B*) WALP*n*/POPC, and (*C*) *X*ALP23/DMPC systems: $\Delta L^{\text{adaptation}} = \langle L_{\text{bilayer}}^{\text{contact}} \rangle - \langle L_{\text{bilayer}}^{\text{bulk}} \rangle$, where $\langle L_{\text{bilayer}}^{\text{contact}} \rangle$ and $\langle L_{\text{bilayer}}^{\text{bulk}} \rangle$ are the average hydrophobic thicknesses of contact and bulk lipid bilayers.

$$\Delta L^{\text{mismatch}} = L_{\text{TM}} \cos\tau - \left\langle L_{\text{bilayer}}^{\text{contact}} \right\rangle,$$

where both L_{TM} and $\langle L_{\text{bilayer}}^{\text{contact}} \rangle$ were calculated in two different ways: one from the simulation trajectory (*solid lines* in Fig. 7) and the other from fixed values (L_{TM} in Table 1 and $\langle L_{\text{bilayer}}^{\text{contact}} \rangle = 23$ Å (DMPC) or 26 Å (POPC); *dotted lines* in Fig. 7). Because L_{TM} remained at nearly the same values as in Table 1 during the simulations, the difference in the two lines represents the influence of the local lipid adaptations on $\Delta L^{\text{mismatch}}$. As shown in Fig. 7 *A*, for WALP16/19, despite the local membrane thinning (Fig. 5 *A*), the negative hydrophobic mismatch is apparent and slightly increases as τ increases (37). Therefore, it becomes clear that the W_{int} contribution is not favorable for tilting of WALP16/19 in DMPC (Fig. 4, *A* and *B*) because of increased deformation of the lipid bilayer as τ increases. In contrast, for WALP23/27, τ at $\Delta L^{\text{mismatch}} \approx 0$ is well matched with τ_{min}, demonstrating that the local lipid adjustments toward $\Delta L^{\text{mismatch}} \approx 0$ (i.e., $\Delta L^{\text{adaptation}} \approx 0$ in Fig. 5 *A*) provide the favorable W_{int} contribution for tilting of WALP23/27 toward τ_{min} (Fig. 4, *C* and *D*) and relieve the deformation stress on the lipid bilayer. At $\tau > \tau_{\text{min}}$, however, bilayer deformation ($\Delta L^{\text{adaptation}} < 0$) causes stress on the lipid bilayer, making the W_{int} contribution unfavorable. While excessive stress on a lipid bilayer at extreme hydrophobic mismatch can induce helix deformations such as helix kink or bending, it also becomes apparent from the thermally accessible tilt regions (Fig. 3 *A* and Table 2) that the membrane bilayer system can tolerate a certain extent of a hydrophobic mismatch by slight lipid adaptations.

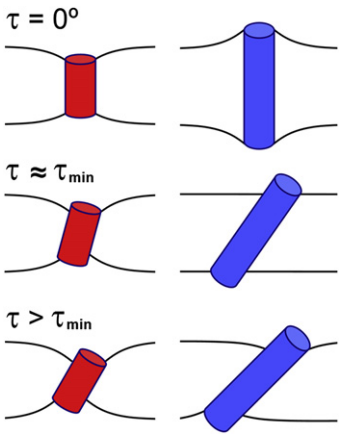

FIGURE 6 Schematic representation of the local lipid adjustment based on the ΔL change (Fig. 5) under negative (*left*) and positive (*right*) hydrophobic mismatch conditions.

As shown in Fig. S1 *A*, the helicity of each helix is well maintained except at energetically unfavorable large τ. The previous study on WALP19 reveals that such helix deformation including helix bending at large τ is attributed to the existence of four Trp anchoring residues at the hydrophobic/hydrophilic interface (18). In other words, it is energetically more favorable for WALP19 to deform the helical conformation slightly at large τ in a DMPC bilayer, than to have Trp side chains inserted into the hydrophobic core (18). Fig. S2 shows the center of mass of each Trp side chain along the Z axis (Z_{Trp}) as a function of τ. Similar to WALP19, Z_{Trp} of WALP16 is around the hydrophobic/hydrophilic interface of the lipid bilayer due to outward-facing of the Trp side chains (see below), despite their relatively short L_{TM}. However, the Trp side chains of WALP23/27 appear to partition into the DMPC hydrophobic core region at large τ. Such difference arises for two reasons. First, because WALP16/19 is under the negative mismatch regardless of τ, the hydrophobic/hydrophilic interfacial matching becomes a dominant factor in optimizing their conformation during helix tilting (in contrast, WALP23/27 gain the favorable W_{int} contribution by optimizing the hydrophobic match, which becomes more dominant than the interfacial matching, at large τ). Second, the rotation angle of each helix during its tilting, determined by the helix-lipid interactions, also dictates the positioning of the Trp residues.

The direction of helix tilting (i.e., rotation angle, ρ) is also an important determinant of TM helix tilting. In our simulations, because the restraint forces are exerted only on the Cα atoms that define the helical principal axis, the helix can rotate around the helical axis, depending on

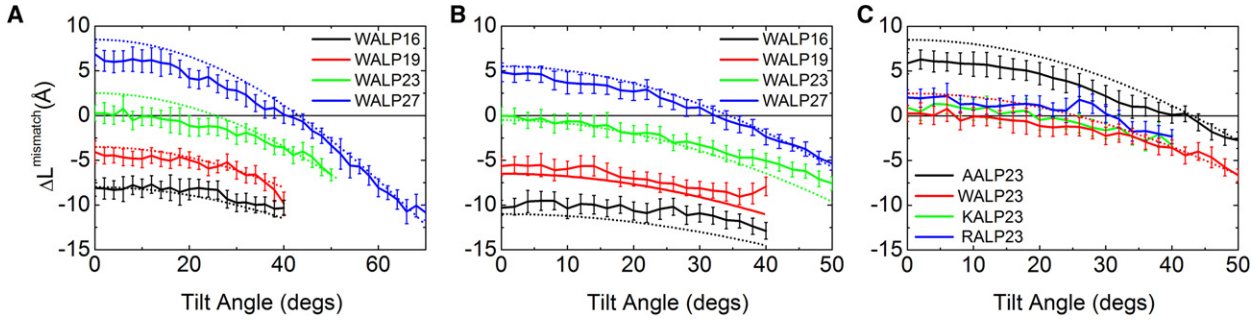

FIGURE 7 Extent of the hydrophobic match ($\Delta L^{\text{mismatch}}$) as a function of τ in (*A*) WALP*n*/DMPC, (*B*) WALP*n*/POPC, and (*C*) *X*ALP23/DMPC systems: $\Delta L^{\text{mismatch}} = L_{\text{TM}}\cos\tau - \langle L_{\text{bilayer}}^{\text{contact}}\rangle$, where L_{TM} is the TM hydrophobic length and $\langle L_{\text{bilayer}}^{\text{contact}}\rangle$ is the average hydrophobic thicknesses of the contact lipids. Both L_{TM} and $\langle L_{\text{bilayer}}^{\text{contact}}\rangle$ were calculated from the simulation trajectory (*solid lines*) or they were set to fixed values (L_{TM} in Table 1 and $\langle L_{\text{bilayer}}^{\text{contact}}\rangle$ = 23 Å (DMPC) or 26 Å (POPC)) (*dotted lines*).

helix-environment (lipid or water) interactions (23). Fig. 8 shows the change of ρ as a function of τ and also illustrates the tilting direction for each WALP*n*/DMPC system. In general, ρ shows large fluctuations at $\tau < 10°$ (due to ill-definition of ρ and low free energy barriers at small tilt angles), but converged to a specific angle with less fluctuation at $\sim\tau_{\text{min}}$. It becomes clear that Z_{Trp} in Fig. S2 is related to the tilting direction. For example, WALP23/27 tilt in a direction between Trp2 and Trp3, so that the Trp residues partition into the membrane hydrophobic region at large τ.

To verify that the helix follows the energetically favorable orientation during the tilting simulations, we have performed additional PMF calculations of WALP23 as a function of τ by restraining ρ at four distinct rotation angles, i.e., $\rho = -150°, -60°, 30°$, and $120°$. As shown in Fig. S3, the tilting energetics is largely dependent on ρ, and the lowest tilting PMF is found with $\rho = 120°$, which corresponds to ρ at $\tau = \tau_{\text{min}}$ ($120.8° \pm 18.5°$) in Fig. 8 *C*. This rotation is also well correlated with $\rho = 155°$ (using our definition) estimated from the solid-state ^{2}H-NMR study (12). Clearly, our results demonstrate that each helix prefers to tilt with a specific rotation based on hydrophobic or interfacial matching, and the helix adopts the energetically favorable orientation during the tilting simulations.

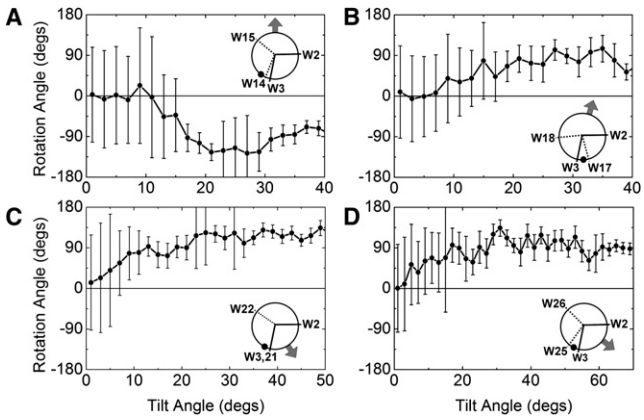

FIGURE 8 TM helix rotation angle (ρ) as a function of τ in (*A*) WALP16, (*B*) WALP19, (*C*) WALP23, and (*D*) WALP27 in DMPC bilayers. The reference atoms, such as Ala^7 (for WALP16), Leu^{10} (for WALP19), and Leu^{14} (for others), and the tilting direction at τ_{min}, are indicated (*solid circles* and *shaded arrows* on the *helical view*), respectively.

Influence of bilayer hydrophobic thickness

In addition to L_{TM}, the TM helix orientation is also affected by L_{bilayer}. Experimental studies have also used various lipid bilayers with different L_{bilayer} to induce different hydrophobic mismatch conditions (12,13). To elucidate the effect of L_{bilayer} on TM helix orientation and lipid adaptations, we used POPC bilayers (L_{bilayer} = ~26 Å) (38) for the PMF calculations and compared the results with those in DMPC. In the WALP*n*/POPC systems, only WALP27 is under the positive mismatch condition at $\tau = 0°$. Similar to the DMPC cases, as shown in Fig. 3 *B* and Table 2, τ_{min} increases and the thermally accessible tilt region becomes wider as L_{TM} increases. However, each TM helix generally shows smaller τ_{min} and $\Delta W(0 \rightarrow \tau_{\text{min}})$, and a broader thermally accessible tilt region than in DMPC, illustrating that the TM helices do respond differently in POPC than in DMPC. The PMF decomposition in Fig. S4 clearly shows that tilting up to τ_{min} is mostly driven by W_{entropy} because all WALP peptides except WALP27 are under the negative mismatch condition in POPC bilayers. The increase in the total PMF after τ_{min} well correlates with W_{int}, but the W_{int} contribution appears to be less significant than in DMPC.

Because of the changes in the hydrophobic mismatch condition and thus in the helix-lipid interaction, the local lipid adjustment of the POPC bilayers is different from that of DMPC. As shown in Fig. 5 *B*, $\Delta L^{\text{adaptation}}$ in POPC generally shows less change than in DMPC for the same L_{TM}. Compared to DMPC, POPC has the same headgroup but a larger cross-sectional area, as the unsaturated acyl chain makes the hydrophobic packing of lipid tails less tight than found in the fully saturated DMPC acyl chains (39). Its more flexible, dynamic nature is attributed to smaller local lipid adaptations in POPC, which, in addition to its larger

$L_{bilayer}$, is sufficient to maximize the hydrophobic match even for WALP27 (Fig. 7 *B*). Hence, the W_{int} contribution to the total PMF provides less additional driving force for WALP27 tilting than in DMPC.

As shown in Fig. S5, most Trp anchoring residues are positioned around the hydrophobic/hydrophilic interface of the POPC bilayers. Only one Trp residue of WALP16 is below the interface because of its relatively short L_{TM} in POPC with larger $L_{bilayer}$. Despite the existence of four Trp anchoring residues at the interface, the WALP*n* peptides do not show any helical deformation (probably due to the flexible nature of POPC acyl chains; see WALP19 in Fig. S1, *A* and *B*, for comparison). Z_{Trp} in Fig. S5 shows only marginal decrease as τ increases, suggesting that the interfacial matching of anchoring residues is dominant throughout TM helix tilting in POPC and thus each helix has broader thermally accessible tilt regions than in DMPC. As shown in Fig. S6, the interfacial matching is closely related to the tilting direction (i.e., rotation angle) having outward-facing of the Trp side chains. Note that the tilting direction is similar for each helix in POPC, but different from that of the WALP*n*/DMPC systems. Such a difference may arise from the different $L_{bilayer}$ in DMPC and POPC bilayers.

Influence of anchoring residues

A flanking residue of a single-pass TM helix can also influence helix tilt and rotation as well as lipid adaptations (12,40). To investigate such influences, we used three different anchoring residues (Ala, Lys, and Arg) in addition to Trp in the WALP23/DMPC system for the PMF calculations. Fig. 3 *C* shows the total PMFs of the *X*ALP23/DMPC (X = A, W, K, and R) systems as a function of τ. Interestingly, even though the *X*ALP23 series have the same L_{TM} except AALP23 (Table 1), their minimum-PMF tilt angles (Table 2) show a direct relationship to the hydrophobicity (41) of its anchoring residues: τ_{min} (RALP23) $<$ τ_{min} (KALP23) $<$ τ_{min} (WALP23) $<$ τ_{min} (AALP23). These results appear to be at odds with the tilt angles estimated from solid-state ^{2}H-NMR experiments (12), showing τ = 4.4° (KALP23) and τ = 5.2° (WALP23). However, it is now apparent that the correct determination of tilt angles using ^{2}H-NMR quadrupolar splitting measurements requires a proper average of rotation angles (16,17,20). For example, as mentioned above, the recent fluorescence spectroscopy experiment (20) shows much larger tilt angle of WALP23 (τ = 24° ± 5°) in a DOPC membrane than the tilt angle (τ = 4.4°~8.2°) estimated from solid-state ^{2}H-NMR measurements (12,13).

The free energy decomposition (Fig. S7) shows that as the hydrophobicity of anchoring residue increases, there is more W_{int} contribution to TM helix tilting up to τ_{min} in addition to the intrinsic $W_{entropy}$ contribution, and the thermally accessible tilt region becomes wider. Such difference is closely related to the local lipid adaptations. As shown in Fig. 5 *C*, $\Delta L^{adaptation}$ disappears around each τ_{min}, and the extent of $\Delta L^{adaptation}$ before τ_{min} is inversely proportional to the hydrophobicity of each anchoring residue. In other words, the W_{int} contribution to TM helix tilting up to τ_{min} arises from the helix-lipid interaction to relieve the hydrophobic mismatch. To avoid exposure of the charged side chains to the hydrophobic membrane interior and to allow them to interact favorably with the aqueous environment (41), as shown in Fig. S8, Lys and Arg anchoring residues prefer to be positioned at 3~5 Å above the hydrophilic/hydrophobic interface where Trp residues are generally positioned. These snorkeling behaviors (14,42) also affect the local lipid adjustment as shown in Figs. 5 *C* and 7 *C*. Consequently, the long charged side chains make a more-dominant interaction with water (Fig. S9), so that they have less τ_{min}.

As shown in Fig. S10, the *X*ALP23/DMPC systems show quite different rotations and thus tilt directions. The large fluctuation in the AALP23 system appears to arise from the flexible dynamics of AALP23 due to a lack of bulky anchoring residue's interaction with membranes. In addition, the large change of ρ and its fluctuation in RALP23 is attributed to the ill-definition of ρ due to slight helix bending at $\tau > 20°$ (Fig. S1 *C*). The tilting direction of KALP23 ($-114.3° \pm 55.8°$) at $\tau = \tau_{min}$ is well correlated with the rotation angle ($\rho = -109°$) estimated from the solid-state ^{2}H-NMR measurement (12). These results demonstrate that the interaction of Lys and Arg anchoring residues at the membrane/water interface plays an important role in determining TM helix orientations.

CONCLUSIONS

To systematically characterize responses of a single-pass TM helix in terms of its orientation (tilt and rotation) and lipid adaptations under various hydrophobic mismatch conditions, we have performed extensive umbrella sampling MD simulations and calculated the PMFs as a function of TM helix tilt angle (τ) in the WALP*n*/DMPC (n = 16, 19, 23, and 27), WALP*n*/POPC, and *X*ALP23/DMPC (X = A, W, K, and R) systems (Table 1 and Table S1). The PMF in each system, its decomposition, and trajectory analysis allow us to generalize such responses and the underlying molecular forces.

1. Tilting of a single-pass TM helix is the major response to a hydrophobic mismatch. Regardless of the negative and positive mismatches, the PMFs in all the systems (Fig. 3 and Table 2) clearly demonstrate that each TM helix prefers to stay around its minimum-PMF tilt angle (τ_{min}) without conformational deformations such as kinks or bending (Fig. S1).
2. Tilting of a single-pass TM helix up to ~10° is inherent. As shown in Fig. 4, Fig. S4, and Fig. S7, there is the intrinsic entropic contribution ($W_{entropy}$) to TM helix tilting in a membrane bilayer, which arises from helix precession around the membrane normal. In other words,

the accessible orientational space of the helix is reduced as τ decreases, which causes the entropy cost associated with small tilt angles. In particular, its cost up to ~10° is high enough to make the TM helix tilt even under negative mismatch conditions, such as WALP16/19 in DMPC bilayers and WALP16/19/23 in POPC bilayers.

3. The favorable helix-lipid interaction provides additional driving forces for TM helix tilting under a positive mismatch. The helix-lipid interactions (W_{int}) are TM sequence- and length-specific, and indeed vary for different mismatch conditions (Fig. 4, Fig. S4, and Fig. S7). Generally, there is no favorable W_{int} contribution under negative mismatch conditions because of increased stress on the (already) perturbed lipid bilayer as τ increases (Figs. 5 and 7). However, under positive mismatch conditions (WALP23/27 in DMPC and WALP27 in POPC), molecular interaction forces, in order to decrease such membrane deformation stress at $\tau < \tau_{min}$, provide additional driving forces to TM helix tilting to τ_{min}.
4. τ_{min} is generally located where there is the hydrophobic match and little or no lipid perturbation under a positive mismatch, as shown in Figs. 5 and 7. It should be stressed that there are the thermally accessible tilt regions of ~10°–20° in single-pass TM helices (Fig. 3 *A* and Table 2) where a certain extent of a hydrophobic mismatch exists. This observation strongly suggests that the membrane system can have some flexibility to tolerate such a mismatch within a certain threshold by slight lipid adaptations.
5. TM helix rotation (ρ) is dependent on the sequence- and length-specific helix-lipid interaction. In other words, ρ is determined by both the anchoring residue type and the mismatch conditions (Fig. 8, Fig. S6, and Fig. S10). As shown in Fig. S3, there is a significant dependence of the tilting energetics on ρ. In general, a single-pass TM helix with bulky anchoring residues can explore various ρ at small τ up to ~10°, but there are significant energy barriers between different ρ regions after $\tau \approx 10°$. The precise estimation of thermally accessible rotation angles as a function of τ further requires the two-dimensional PMF calculations as a function of both τ and ρ.
6. Anchoring residues at the hydrophilic/hydrophobic interface can be an important determinant of TM helix orientation. As shown in Fig. S2, Fig. S5, and Fig. S8, it is apparent that anchoring residues, such as Arg, Lys, and Trp, prefer to position at the hydrophilic (lipid headgroup and water)/hydrophobic interface at ~τ_{min}, regardless of the negative and positive mismatches. In general, there are no other favorable interactions available in the systems under negative mismatch conditions, and thus such interfacial matching appears to be more important. Interestingly, τ_{min} in the *X*ALP23/DMPC systems (Table 2) has a direct relationship to the hydrophobicity of its anchoring residues: τ_{min} (RALP23) < τ_{min} (KALP23) < τ_{min} (WALP23) < τ_{min} (AALP23) (i.e., the more hydrophobic the anchoring residue, the more the TM helix prefers to tilt).

This generalization, based on the extensive PMF calculations and trajectory analysis, provides in-depth insights into the responses of the single-pass TM helix and lipid bilayers to various hydrophobic mismatches. These findings are particularly important because of the abundance of membrane proteins with a single-pass TM helix and their association and conformational changes involved in TM-induced signaling (6,7). Yet, we need further investigation on the influence of the TM helix-helix interaction on the structure and function of these biologically important systems.

SUPPORTING MATERIAL

One table and 10 figures are available at http://www.biophysj.org/biophysj/supplemental/S0006-3495(10)00478-9.

We are grateful to Jinhyuk Lee for initial efforts on this work and to Sunhwan Jo and Huan Rui for helpful comments on the manuscript.

This work was supported by National Science Foundation grant No. MCB-0918374. This research was also supported in part by the National Science Foundation (No. OCI-0503992) through TeraGrid resources provided by Purdue University.

REFERENCES

1. Andersen, O. S., and R. E. Koeppe, 2nd. 2007. Bilayer thickness and membrane protein function: an energetic perspective. *Annu. Rev. Biophys. Biomol. Struct.* 36:107–130.
2. Killian, J. A. 1998. Hydrophobic mismatch between proteins and lipids in membranes. *Biochim. Biophys. Acta.* 1376:401–415.
3. Pelham, H. R. B., and S. Munro. 1993. Sorting of membrane proteins in the secretory pathway. *Cell.* 75:603–605.
4. Johannsson, A., G. A. Smith, and J. C. Metcalfe. 1981. The effect of bilayer thickness on the activity of ($Na^+ + K^+$)-ATPase. *Biochim. Biophys. Acta Biomembr.* 641:416–421.
5. Froud, R. J., C. R. A. Earl, …, A. G. Lee. 1986. Effects of lipid fatty acyl chain structure on the activity of the ($Ca^{2+} + Mg^{2+}$)-ATPase. *Biochim. Biophys. Acta Biomembr.* 860:354–360.
6. Arkin, I. T., A. T. Brünger, and D. M. Engelman. 1997. Are there dominant membrane protein families with a given number of helices? *Proteins: Struct. Funct. Gen.* 28:465–466.
7. Lichanska, A. M., and M. J. Waters. 2008. New insights into growth hormone receptor function and clinical implications. *Hormone Res Paed.* 69:138–145.
8. van der Wel, P. C. A., E. Strandberg, …, R. E. Koeppe, 2nd. 2002. Geometry and intrinsic tilt of a tryptophan-anchored transmembrane α-helix determined by ^{2}H NMR. *Biophys. J.* 83:1479–1488.
9. Park, S. H., and S. J. Opella. 2005. Tilt angle of a trans-membrane helix is determined by hydrophobic mismatch. *J. Mol. Biol.* 350:310–318.
10. de Planque, M. R. R., and J. A. Killian. 2003. Protein-lipid interactions studied with designed transmembrane peptides: role of hydrophobic matching and interfacial anchoring. *Mol. Membr. Biol.* 20:271–284, (Review).
11. Killian, J. A., and T. K. Nyholm. 2006. Peptides in lipid bilayers: the power of simple models. *Curr. Opin. Struct. Biol.* 16:473–479.

12. Ozdirekcan, S., D. T. S. Rijkers, …, J. A. Killian. 2004. Influence of flanking residues on tilt and rotation angles of transmembrane peptides in lipid bilayers. A solid-state ^{2}H NMR study. *Biochemistry*. 44:1004–1012.

13. Strandberg, E., S. Ozdirekcan, …, J. A. Killian. 2004. Tilt angles of transmembrane model peptides in oriented and non-oriented lipid bilayers as determined by ^{2}H solid-state NMR. *Biophys. J*. 86:3709–3721.

14. Kandasamy, S. K., and R. G. Larson. 2006. Molecular dynamics simulations of model trans-membrane peptides in lipid bilayers: a systematic investigation of hydrophobic mismatch. *Biophys. J*. 90:2326–2343.

15. Petrache, H. I., D. M. Zuckerman, …, T. B. Woolf. 2002. Hydrophobic matching mechanism investigated by molecular dynamics simulations. *Langmuir*. 18:1340–1351.

16. Ozdirekcan, S., C. Etchebest, …, P. F. Fuchs. 2007. On the orientation of a designed transmembrane peptide: toward the right tilt angle? *J. Am. Chem. Soc*. 129:15174–15181.

17. Esteban-Martín, S., and J. Salgado. 2007. The dynamic orientation of membrane-bound peptides: bridging simulations and experiments. *Biophys. J*. 93:4278–4288.

18. Lee, J., and W. Im. 2008. Transmembrane helix tilting: insights from calculating the potential of mean force. *Phys. Rev. Lett*. 100:018103.

19. Im, W., and C. L. Brooks, 3rd. 2005. Interfacial folding and membrane insertion of designed peptides studied by molecular dynamics simulations. *Proc. Natl. Acad. Sci. USA*. 102:6771–6776.

20. Holt, A., R. B. M. Koehorst, …, J. A. Killian. 2009. Tilt and rotation angles of a transmembrane model peptide as studied by fluorescence spectroscopy. *Biophys. J*. 97:2258–2266.

21. Torrie, G. M., and J. P. Valleau. 1977. Nonphysical sampling distributions in Monte Carlo free-energy estimation: umbrella sampling. *J. Comp. Phys*. 23:187–199.

22. Lee, J., and W. Im. 2007. Restraint potential and free energy decomposition formalism for helical tilting. *Chem. Phys. Lett*. 441:132–135.

23. Lee, J., and W. Im. 2007. Implementation and application of helix-helix distance and crossing angle restraint potentials. *J. Comput. Chem*. 28:669–680.

24. Im, W., J. Lee, …, H. Rui. 2009. Novel free energy calculations to explore mechanisms and energetics of membrane protein structure and function. *J. Comput. Chem*. 30:1622–1633.

25. Jo, S., J. B. Lim, …, W. Im. 2009. CHARMM-GUI Membrane Builder for mixed bilayers and its application to yeast membranes. *Biophys. J*. 97:50–58.

26. Jo, S., T. Kim, and W. Im. 2007. Automated builder and database of protein/membrane complexes for molecular dynamics simulations. *PLoS One*. 2:e880.

27. Jo, S., T. Kim, …, W. Im. 2008. CHARMM-GUI: a web-based graphical user interface for CHARMM. *J. Comput. Chem*. 29:1859–1865.

28. Brooks, B. R., C. L. Brooks, 3rd, …, M. Karplus. 2009. CHARMM: the biomolecular simulation program. *J. Comput. Chem*. 30:1545–1614.

29. MacKerell, Jr., A. D., D. Bashford, …, M. Karplus. 1998. All-atom empirical potential for molecular modeling and dynamics studies of proteins. *J. Phys. Chem. B*. 102:3586–3616.

30. Mackerell, Jr., A. D., M. Feig, and C. L. Brooks, 3rd. 2004. Extending the treatment of backbone energetics in protein force fields: limitations of gas-phase quantum mechanics in reproducing protein conformational distributions in molecular dynamics simulations. *J. Comput. Chem*. 25:1400–1415.

31. Jorgensen, W. L., J. Chandrasekhar, …, M. L. Klein. 1983. Comparison of simple potential functions for simulating liquid water. *J. Chem. Phys*. 79:926–935.

32. Klauda, J. B., B. R. Brooks, …, R. W. Pastor. 2005. An ab initio study on the torsional surface of alkanes and its effect on molecular simulations of alkanes and a DPPC bilayer. *J. Phys. Chem. B*. 109:5300–5311.

33. Nagle, J. F., and S. Tristram-Nagle. 2000. Structure of lipid bilayers. *Biochim. Biophys. Acta Gene Struct. Expression*. 1469:159–195.

34. Ryckaert, J.-P., G. Ciccotti, and H. J. C. Berendsen. 1977. Numerical integration of the Cartesian equations of motion of a system with constraints: molecular dynamics of *n*-alkanes. *J. Comp. Phys*. 23:327–341.

35. Hoover, W. G. 1985. Canonical dynamics: equilibrium phase-space distributions. *Phys. Rev. A: At. Mol. Opt. Phys*. 31:1695–1697.

36. Feller, S. E., Y. Zhang, …, B. R. Brooks. 1995. Constant pressure molecular dynamics simulation: the Langevin piston method. *J. Chem. Phys*. 103:4613–4621.

37. Weiss, T. M., P. C. A. van der Wel, …, H. W. Huang. 2003. Hydrophobic mismatch between helices and lipid bilayers. *Biophys. J*. 84:379–385.

38. Nezil, F. A., and M. Bloom. 1992. Combined influence of cholesterol and synthetic amphiphilic peptides upon bilayer thickness in model membranes. *Biophys. J*. 61:1176–1183.

39. Róg, T., K. Murzyn, …, M. Pasenkiewicz-Gierula. 2004. Effects of phospholipid unsaturation on the bilayer nonpolar region: a molecular simulation study. *J. Lipid Res*. 45:326–336.

40. de Planque, M. R. R., J.-W. P. Boots, …, J. A. Killian. 2002. The effects of hydrophobic mismatch between phosphatidylcholine bilayers and transmembrane α-helical peptides depend on the nature of interfacially exposed aromatic and charged residues. *Biochemistry*. 41:8396–8404.

41. Wimley, W. C., and S. H. White. 1996. Experimentally determined hydrophobicity scale for proteins at membrane interfaces. *Nat. Struct. Mol. Biol*. 3:842–848.

42. Strandberg, E., and J. A. Killian. 2003. Snorkeling of lysine side chains in transmembrane helices: how easy can it get? *FEBS Lett*. 544:69–73.